Heliyon 9 (2023) e22877

Contents lists available at ScienceDirect

Heliyon

journal homepage: www.cell.com/heliyon

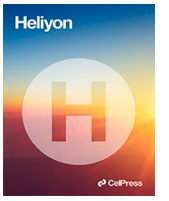

A novel phosphorus-nitrogen-based hyperbranched polysiloxane for improving the fire safety of PA6 with suppressed melt droplets and good mechanical properties

Shuo Fan [a,b,c,*], Jinhao Zeng [a,b], Peng Yang [a,b], Meijia Cheng [a]

[a] College of Textile Science and Engineering (International Institute of Silk), Zhejiang Sci-Tech University, Hangzhou, Zhejiang Province, 310018, China
[b] Zhejiang Sci-tech University Tongxiang Research Institute, Tongxiang, Zhejiang Province, China
[c] School of Chemical and Material Engineering, Jiangnan University, Wuxi, Jiangsu, 214122, China

ARTICLE INFO

Keywords:
Polyamide 6
Hyperbranched polysiloxane
Melt droplets
Mechanical properties

ABSTRACT

The combustible defects of polyamide 6 (PA6), especially the flammable melt-dripping behavior, have greatly limited its application in some particular fields. In this work, a halogen-free hyperbranched polysiloxane (PBDSi) containing DOPO and Schiff base was designed via Michael's addition reaction and dehydration-condensation reaction. Results showed that the char yield (Y_c) of PBDSi attained 37.9 wt%, confirming the satisfactory charring behavior of PBDSi for preparing flame-retardant PA6. Just by adding 3 wt% of PBDSi, the serious melt droplets of PA6 were suppressed effectively. The prepared PA6/PBDSi-3 with 5 wt% of PBDSi could achieve the highest value of limited oxygen index (LOI) of 27.2 %, while that of PA6 is 21.0 %. Meanwhile, PA6/PBDSi-3 obtained an apparent reduction in the peak heat release rate (PHRR) value of 31.1 % compared with pure PA6. The cooperated effect of DOPO, Schiff base, and polysiloxane that contributed to generating a silicon-phosphorous-rich char layer and releasing incombustible volatiles that were determined to be the essential factor for the improved fire safety of PA6/PBDSi were explored intensively. Inspiringly, PA6/PBDSi composites exhibited a slight mechanical loss concerning PA6, overcoming the great challenge of developing additive flame-retardant materials to balance mechanical properties and fire safety.

1. Introduction

Polyamide 6 (PA6) as an indispensable material is widely used in the textile, aerospace, and packaging fields. However, the severe fire risk of fast burning speed, high heat release, and terrible melt droplets for PA6 dramatically limit the application of PA6 in some particular fields [1,2]. Especially the melt droplets, even if they effectively stop the burning of materials by removing heat quickly, they pose an enormous threat in causing scalding and extending the fire-spreading area. Therefore, the flame-retardant modification of PA6 for good anti-dripping behavior simultaneously is still of great challenge.

Considering the features of convenience, efficiency, and easy processability, melt-blending is the most popular method for fabricating flame-retardant materials. Up to now, a variety of halogen-free flame retardants, such as intumescent flame retardants [3],

* Corresponding author. College of Textile Science and Engineering (International Institute of Silk), Zhejiang Sci-Tech University, Hangzhou, Zhejiang Province, 201620, China.
E-mail address: fs2020@zstu.edu.cn (S. Fan).

https://doi.org/10.1016/j.heliyon.2023.e22877
Received 15 August 2023; Received in revised form 6 October 2023; Accepted 22 November 2023
Available online 27 November 2023

graphene [4], phosphorus [5], and silicon flame retardants [6], have been developed for flame-retardant PA6 with a satisfactory anti-dripping behavior. Nevertheless, flame-retardant additives, mainly inorganic additives, invariably cause serious physical deterioration of the modified matrix owing to the large particle size, poor dispersion, and high addition of these additives [7]. The tricky problem of achieving a balance between less mechanical loss and higher fire safety of the modified matrix still exists, and how to work out the problem above is another challenge in developing flame-retardant PA6.

In this case, organic polysiloxane, with non-toxicity, excellent thermal stability, and good interfacial compatibility, is a promising halogen-free flame retardant [8,9]. In the combustion process, the pyrolysis silicon fragments can form a stable carbonaceous-silicate layer to insulate the matrix from heat and combustible gases and restrain the melt droplets of the matrix [10,11]. Cai et al. [12,13] and Hsieh et al. [14] have synthesized two hyperbranched polysiloxanes (HPSi, PSiN) and benzoxazine-containing polysiloxanes, respectively. These organic polysiloxanes reduce the fire risk of the matrix materials efficiently. In our previous studies [15], a Schiff base-based organic polysiloxane was also designed. With the unique C═N structure, the Schiff base unit can cause a self-crosslinking reaction at a lower temperature and strengthen the formed carbonaceous-silicate layer [16,17]. This prepared polysiloxane of PCNSi significantly improves the anti-dripping behavior of PA6. Moreover, the PCNSi exhibits good interfacial compatibility with the PA6 matrix, and a relatively small mechanical loss is achieved for the modified PA6 in relation to PA6, which conquers the great defects of the majority of additive flame retardants. However, it is unfortunate that satisfactory flame retardancy is hard for the matrix when the PCNSi is used alone with a small content according to the defective flame-retardant function of organic polysiloxane. As the addition of PCNSi is 6 wt%, the LOI value of PA6/PCNSi-3 is only 24.9 %. In general, polysiloxane typically works on the condensed phase rather than the gas phase in the combustion process. Therefore, a synergistic agent that powerfully works as a reinforcer in the gas phase is urgently necessary to develop polysiloxane-based flame retardants.

Phosphorus, as an eco-friendly flame retardant, is widespread in flame-retardant modification, which possesses the capacity to quench the pyrolysis free radicals and promote carbonaceous layer formation in the gases and condensed phase, respectively [18]. These merits neatly can make up for the deficiencies of polysiloxane, and phosphorus is thus considered a suitable synergistic candidate. Now, several phosphorus-silicon synergistic flame retardants have been designed. Representative works include a P–N–Si polymeric flame retardant by Wang [19], a polyborosiloxane microencapsulated ammonium polyphosphate by Ran [20], and a polydimethylsiloxane-wrapped aluminum diethylphosphinate flame retardant by Pan [21]. Therein, 9, 10-Dihydro-9-oxa-10phosphaphenanthrene-10-oxide (DOPO) is a well-established organic phosphorus flame retardant, which can act as both gas and acid source in intumescent flame retardants [22–24]. A series of DOPO-silicon flame retardants are reported. Wang [25] synthesizes two novel DOPO-silicon flame retardants of PSAP and DPP-Si, and the LOI of epoxy containing 15 wt% of either DPP-Si or PSAP can reach 27.6 %. J. Sahyoun group [26] designs an organophosphorus alkoxysilane (SiDOPO), and a reduction of 33 % for the peak of heat release rate (PHRR) is achieved for the modified PA66/PA6 copolymer with 10 wt% content of SiDOPO. In addition, He [27] prepares two phosphonate oligomers containing Schiff-base units (PSA, POSC), and the PA6-PSA20 and PA6-POSC20 composite achieve the LOI of 27 % and 32 %.

Based on the above works, the synergistic flame-retardant functions of DOPO with polysiloxane or Schiff-base for PA6-based materials can be supposed. In this study, a hyperbranched polysiloxane (PBDSi) containing DOPO and Schiff base is synthesized via Michael addition reaction and dehydration-condensation to build a "gas-condensed phase" flame-retardant system. Then, the PBDSi is blended into PA6 matix to prepare flame-retardant PA6/PBDSi composites by the melt-blending method. Thermal stability, combustion behavior, and mechanical properties of PA6/PBDSi composite are investigated systematically, and the possible flame-retardant working mode of PBDSi is then proposed and illustrated.

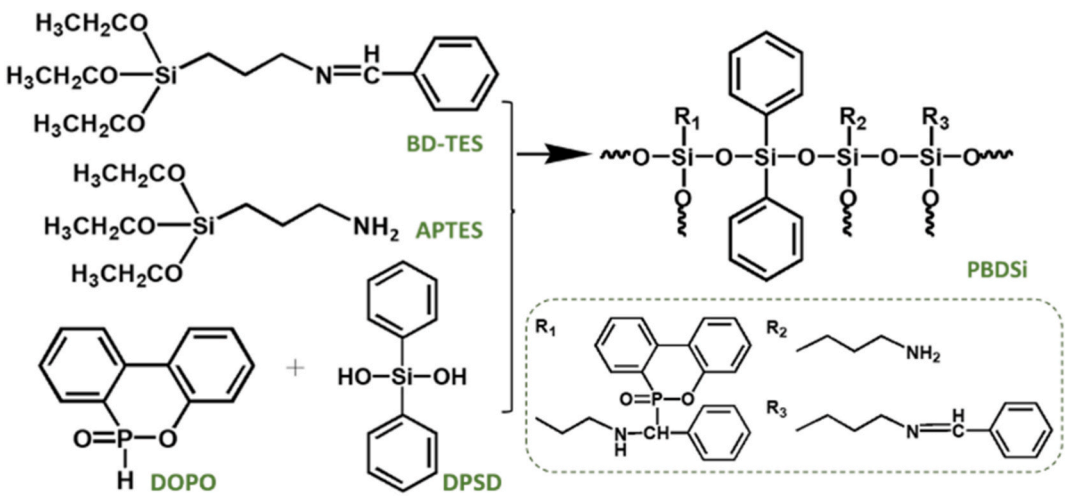

Fig. 1. The synthesis route of PBDSi.

2. Experiment

2.1. Materials

3-aminopropyl triethoxysilane (APTES, 98 %), diphenylsilanediol (DPSD, 98 %), DOPO (97 %), and benzaldehyde (AR, 98.5 %) were from Sinopharm Chemical Reagent Co., Ltd (Beijing, China). Anhydrous ethanol (99.7 %) was from Shanghai Macklin Biochemical Technology Co., Ltd. (Shanghai, China). PA6 pellets were from Yuyao Chihong Plastics Co., Ltd. (Zhejiang, China).

2.2. Synthesis of PBDSi

PBDSi was synthesized via a dehydration condensation reaction. In detail, 200 mL of anhydrous ethanol, 100 mL of Schiff base-contained triethoxysilane solution (BD-TES, 0.050 mol, Fig. S1), 2.7g (0.0125 mol) of DPSD and 9.2 g (0.0425 mol) of DOPO were mixed in a three-necked flask. The flask was equipped with a magnetic stirrer and a reflux condenser. Afterwards, the mixture was purged by nitrogen for air replacement and then heated to 80 °C for the reaction of 8 h. Finally, the mixture was cooled to room temperature, and the product of PBDSi was achieved after drying in a vacuum. The route of synthesizing PBDSi is shown in Fig. 1.

2.3. Preparation of PA6/PBDSi composites

The PA6 pellets were blended with PBDSi using a twin-screw extruder. Before blending, all pellets were dried in a tumbling drier at 120 °C for 12 h. Finally, PA6/PBDSi composites (PA6/PBDSi-1, PA6/PBDSi-2, and PA6/PBDSi-3) were prepared according to the 1 %, 3 %, and 5 % weight ratio. Table 1 lists the composition of the prepared PA6/PBDSi composites.

2.4. Characterization

Fourier transform infrared (FTIR) spectrum was collected on a Nicolet 6700 Spectrometer (Thermo Fisher, USA). Wavenumbers range is 400–4000 cm^{-1}.

Nuclear magnetic resonance (^{1}H NMR and ^{29}Si NMR) spectrum was recorded by a Bruker AVANCE III HD 600 MHz Spectrometer (Bruker, USA). The deuterated solvent is DMSO (*d*6).

The degree of branching (DB) value of the hyperbranched structure of polymers was determined by Frechet's equation:

$$DB = \frac{(\mathrm{D} + \mathrm{T})}{(D + T + L)} \times 100\%$$

L is linear structure; T is terminal structure; D is dendritic structure.

Differential scanning calorimetry (DSC) curve was obtained from a PerkinElmer DSC 4000 instrument (PerkinElmer, USA). Firstly, a 6 ± 0.5 mg tested sample was heated to 250 °C under the heating rate of 20 °C·min^{-1}. Afterwards, the sample remained in isothermal conditions at 250 °C for 3 min and then cooled to 20 °C. Finally, the sample was reheated to 270 °C under the heating rate of 10 °C·min^{-1}. The whole process is in a nitrogen atmosphere.

The degree of crystallinity (X_c) was calculated according to the equation:

$$X_c = \frac{\Delta H_m}{\Delta H_m^*} \times 100\%$$

ΔH_m is the melting enthalpy of the tested PA6; ΔH_m* is the melting enthalpy of PA6 with complete crystallization, 190.6 J g^{-1}.

Thermogravimetric analysis (TGA) curves were recorded on a PerkinElmer 4000 instrument (PerkinElmer, USA). A 7 ± 0.5 mg tested sample was directly heated from 30 to 700 °C under the heating rate of 10 °C·min^{-1}.

Microscale combustion colorimeter (MCC) test was conducted with PX-01-008 colorimeter (Suzhou Phinix Instrument Co., Ltd., China) to study the heat release behavior of samples, ASTM D7309-11. 8 mg of sample was heated from 30 to 800 °C under the heating rate of 1 °C s^{-1}. The total heat release (THR) values were calculated by the heat release rate (HRR) curve.

Limiting oxygen index (LOI) test was carried out on a ZR-01 instrument (Qingdao Ruixinjie Instrument Co., Ltd., China) with a sample dimension of 100 × 10 × 4 mm^3, ASTM D 2863.

The tensile test was measured on a universal testing machine 68TM Series in accordance with GB/T 1040.2–2018. The samples were processed into a dumbbell shape with 150 × 10 × 4 mm^3 dimensions. The impact strength was tested in ST-XBL-5.5D Digital

Table 1
Thermal properties of PA6 and PA6/PBDSi composites.

Sample	PA6 (wt%)	PBDSi (wt%)	T_m (°C)	X_c (%)	Nitrogen atmosphere			Air atmosphere		
					$T_{5\%}$ (°C)	T_{max} (°C)	Y_c (wt%)	$T_{5\%}$ (°C)	T_{max} (°C)	Y_c (wt%)
PA6	100	–	220	24.5	393	468	0.2	380	451	0.1
PA6/PBDSi-1	100	1	218	23.8	332	400	2.6	325	397	2.1
PA6/PBDSi-2	100	3	214	23.2	313	408	5.3	310	403	6.3
PA6/PBDSi-3	100	5	208	21.3	318	390	7.4	317	380	8.5

IZOD Impact Tester according to GB/T 1843–2008 with a 5.5 J, and the dimension of the sample was 80 × 10 × 4 mm^3.

Scanning electron microscopy (SEM) was performed in a VEGA3 GMH/GMU SEM instrument (Tescan, Czech Republic).

Raman spectra were recorded on a LabRam HR Evolution instrument (HORIBA, France), $\lambda = 532$ nm.

X-ray photoelectron spectroscopy (XPS) was measured in an Escalab 250Xi spectrometer (Thermo Fisher, USA). Al-Kα excitation radiation, h$\upsilon = 1361.0$ eV.

Pyrolysis-gas chromatography/mass spectrometry (Py-GC/MS) was collected on a GC/MS-QP-2010 Ultra spectrometer (Shimadzu, Japan).

Thermogravimetric analysis-infrared spectrometry (TG-IR) spectrum was conducted in STA 449 F5 analyzer (NETZSCH, Germany). The samples were heated from 30 to 650 °C with a heating rate of 10 °C·min^{-1} in a nitrogen atmosphere. Wavenumbers range is 600–4000 cm^{-1}.

3. Results and discussion

3.1. Characterization of PBDSi

FTIR and NMR characterize the chemical structures of PBDSi. As shown in the FTIR spectrum of PBDSi from Fig. 2(a), the characteristic peak of P–H at 2433 cm^{-1} belonging to DOPO units disappears, indicating the Michael addition reaction occurs between the Schiff base and DOPO. Meanwhile, a broad absorption peak assigned to the stretching vibration of Si–O–Si at 1053 cm^{-1} is observed from the FTIR spectrum of PBDSi, while the absorption peak at 3200 cm^{-1} of the hydroxyl group attached to silicon atoms (Si–OH) originated from DPSD almost disappears distinctly, which suggests that BD-TES reacts with DPSD via a dehydration condensation reaction. Moreover, the peak at 1645 cm^{-1} assigned to C═N still exists in the FTIR spectrum of PBDSi. These results show strong evidence that the branched polysiloxane containing Schiff base and DOPO unit is prepared successfully [28,29]. The chemical structure of PBDSi is further confirmed by the results from ^{1}H NMR in Fig. 2 (b). Herein, the signals in 7.0–7.9 ppm belonging to the phenyl group (Ar–H) from DPSD and DOPO structure, and the chemical shifts (–CH–, $–CH_2–$) at (a) 4.37, (c) 8.02, (d) 3.53, (e) 1.71, and (f) 0.58 ppm, appear as expected.

^{29}Si NMR is then applied to determine the hyperbranched structure of PBDSi. In Fig. 2(c), three resonance peaks resulting from the 3 + 3 + 2 condensation polymerization are observed at $\delta = -48$ ppm, $\delta = -60$ ppm and $\delta = -67$ ppm, which can be assigned to the silicon in the D_2, T_2, and T_3 structures of [–Si$(OSi)_2$], [–Si(OH) $(OSi)_2$], and [–Si$(OSi)_3$], respectively. As reported [30,31], the DB value

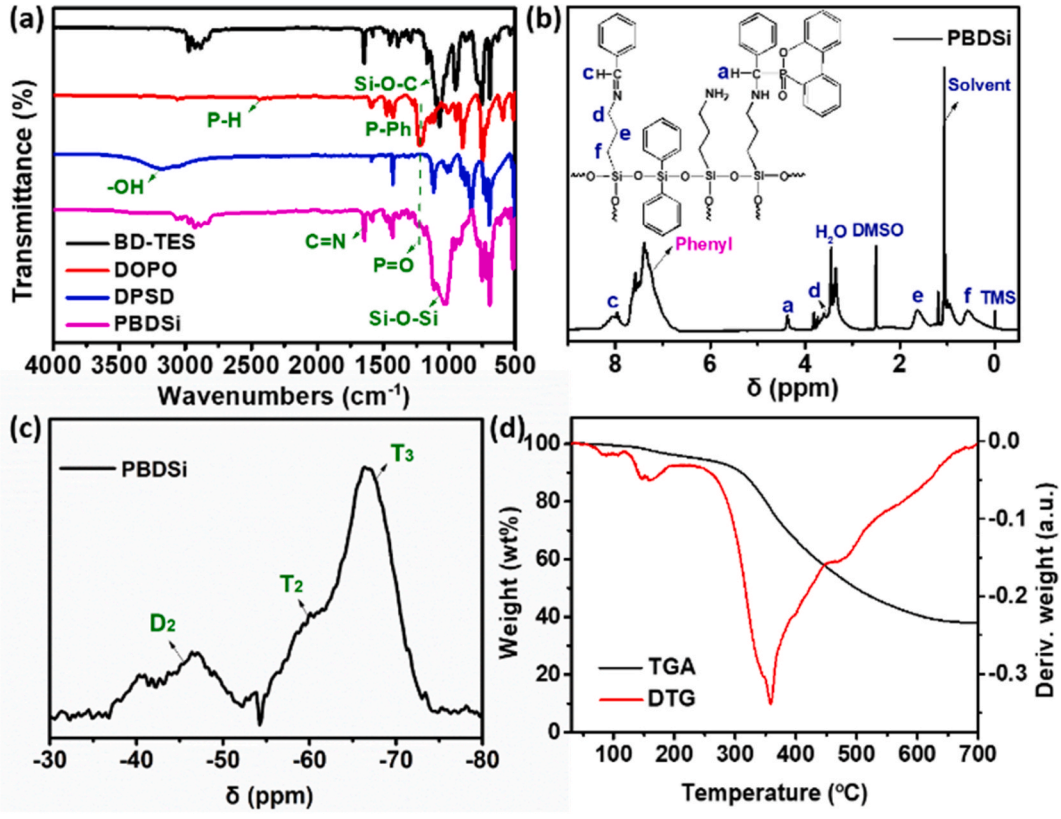

Fig. 2. (a) FTIR spectra of BD-TES, DOPO, DPSD, and PBDSi, (b) ^{1}H NMR and (c) ^{29}Si NMR spectra, and (d) TGA curve of PBDSi in a nitrogen atmosphere.

is the essential index for assessing the hyperbranched structure of polymers. Accordingly, D_2, T_2, and T_3 are classified as linear (L), terminal (T), and dendritic (D) structures, and the DB value of PBDSi is determined to be 0.81 via calculating the ^{29}Si-NMR. This DB value of PBDSi is higher than other conventional hyperbranched polymers.

TGA is carried out to explore the thermal properties of PBDSi. As shown in the TGA curve under a nitrogen atmosphere of PBDSi (Fig. 2 (d)), the initial degradation temperature ($T_{5\%}$) and char yield (Y_c) of PBDSi is 237 °C and 37.9 wt%, respectively. This result confirms that PBDSi presents satisfactory thermal stability and charring behavior for preparing flame-retardant PA6.

3.2. Interfacial morphology and thermal properties of PA6/PBDSi composites

Generally, interfacial compatibility plays a crucial action in the inherent properties of composites, and mechanical properties in particular. SEM is thus adopted to monitor the interfacial compatibility between PBDSi and PA6. The correlated SEM images of the fracture section for PA6 and PA6/PBDSi are displayed in Fig. 3. It is apparent that almost no difference is observed among PA6 and PA6/PBDSi, and all samples exhibit an analogous homogenous phase, which reflects the good interfacial compatibility in PA6/PBDSi composite.

The thermal properties of PA6 and PA6/PBDSi are studied. According to the DSC curves in Fig. 4(a), a reduction of approximately 10 °C in the melting temperature (T_m) is obtained for PA6/PBDSi composites compared with PA6. In addition, the X_c values of composites are calculated in Table 1. It is seen that the X_c values of PA6/PBDSi composites also decrease gradually as the amount of PBDSi increases, explicitly suggesting the negative impact of PBDSi on the crystallization behavior of PA6. Meanwhile, it is seen that multiple melting peaks are observed for PA6/PBDSi composites. According to reports [32], the above result is probably ascribed to the co-existence of good crystallization and incomplete crystallization in composites.

As shown in Fig. 4(b), a remarkable reduction of approximately 60–80 °C for the $T_{5\%}$ values is observed for PA6/PBDSi by comparing the TGA curves of PA6 and PA6/PBDSi in a nitrogen atmosphere, which is mainly ascribed to the prior degradation of PBDSi. Conversely, the Y_c value of PA6/PBDSi composites increases when rising the addition of PBDSi. PA6/PBDSi-3 reaches the highest Y_c value of 7.4 wt%, much higher than the Y_c values of PA6 of 0.2 wt%. Meanwhile, it is noteworthy that a similar variation is also observed in the TGA curves under the air atmosphere (Fig. 4(c)). The Y_c value of PA6/PBDSi-3 approaches 8.5 wt%, while the Y_c value of PA6 is only 0.1 wt%. These inspiring increased Y_c values indicate the positive function of PBDSi on improving the char-forming capacity of PA6. Generally, the formed char residue is an excellent protective barrier for insulating the matrix from oxygen and heat [33,34].

3.3. Mechanical properties

The tensile and impact strength of samples are evaluated, and the relevant data are summarized in Fig. 4(d) and Fig. S2. It is seen

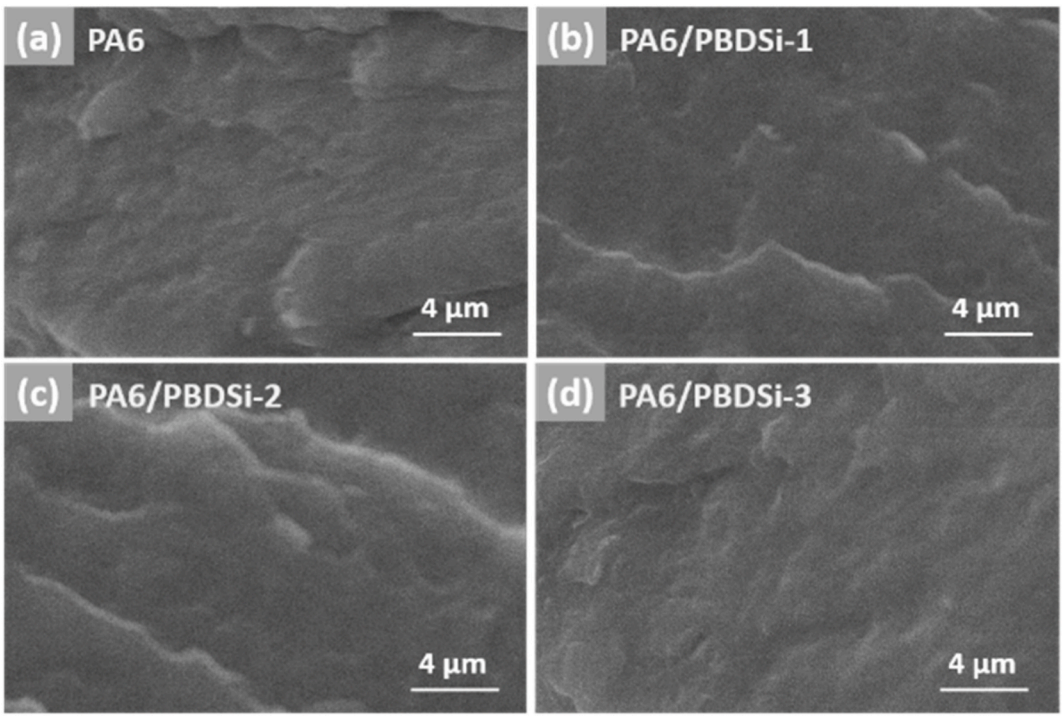

Fig. 3. SEM images of fracture sections for (a) PA6, (b) PA6/PBDSi-1, (c) PA6/PBDSi-2 and (d) PA6/PBDSi-3.

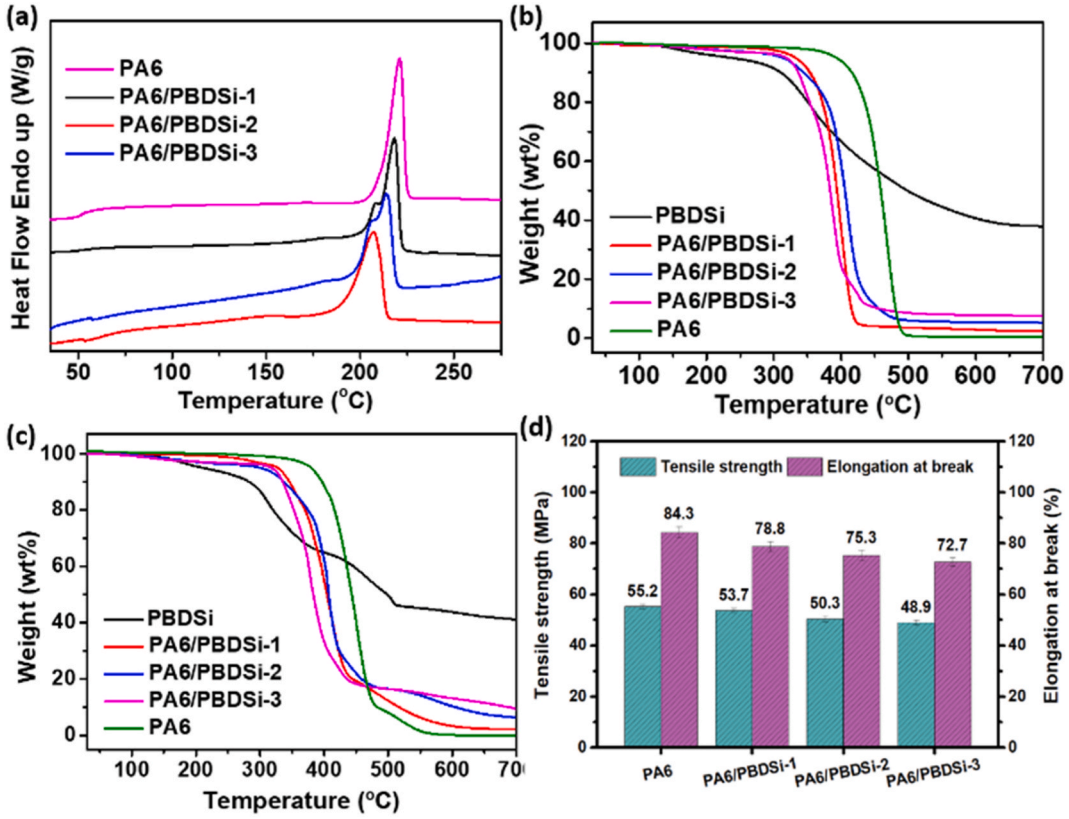

Fig. 4. (a) DSC, (b) TGA (nitrogen atmosphere), (c) TGA (air atmosphere) curves, and (d) Mechanical properties of PA6 and PA6/PBDSi composites.

that a relatively small decrease is observed for both tensile and impact strength of PA6/PBDSi composites. PA6/PBDSi-3 maintains the value of tensile and impact strength of 48.9 MPa and 4.15 kJ/m^2, respectively, which are close to these values of 55.2 MPa and 4.57 kJ/m^2 of PA6. These results may be closely related to the lower addition of flame retardant and good interfacial compatibility in PA6/PBDSi composites.

3.4. Combustion behaviors

LOI, as a typical method, is applied to explore the ignition behavior of PA6 and its composites and the related data are displayed in Table 2. The LOI value enormously increases to 27.2 % for PA6/PBDSi-3 with 5 wt% content of PBDSi from 21.0 % for PA6. Moreover, the melt droplets of PA6/PBDSi-2 are suppressed completely during combustion as only 3 wt% of PBDSi is added, whereas PA6 burns quickly with serious flaming melt droplets produced. These results determine the cheerful efficiency of PBDSi in increasing the fire safety of PA6, especially in anti-dripping behavior.

MCC is utilized to directly evaluate the heat-release properties of PA6 and PA6/PBDSi. HRR curves are shown in Fig. 5. PA6 and PA6/PBDSi present the same single peak in HRR curves, but the ignition temperature of PA6/PBDSi is earlier than that of PA6 due to the preferential thermal degradation of PBDSi. Meanwhile, there is also a remarkable reduction of approximately 60 °C for the temperature at PHRR (T_{peak}) of PA6/PBDSi compared with PA6. This variation trend is consistent with the thermal degradation change of PA6 composites. Conversely, a continuous reduction for the PHRR of PA6/PBDSi composites is attained with the increasing addition of PBDSi. In particular, when the amount of PBDSi reaches 5 wt%, the maximum reduction in the PHRR value of 31.1 % is achieved for PA6/PBDSi-3. In general, PHRR is critical to assessing the fire risk of materials, and a lower PHRR is an indication of a lower fire risk [35,36]. According to the results of THR values from Table 2, there is still a distinct decrease of PA6/PBDSi in the THR values when

Table 2
The combustion data for PA6 and PA6/PBDSi composites.

Sample	LOI (%)	Dripping[a]	PHRR (W/g)	T_{peak} (°C)	THR (kJ/g)
PA6	21.0 ± 0.2	Yes	990.3	465.0	27.8
PA6/PBDSi-1	21.0 ± 0.2	Yes	917.2	416.1	23.3
PA6/PBDSi-2	25.7 ± 0.1	No	761.1	405.8	22.2
PA6/PBDSi-3	27.2 ± 0.2	No	682.2	403.4	22.0

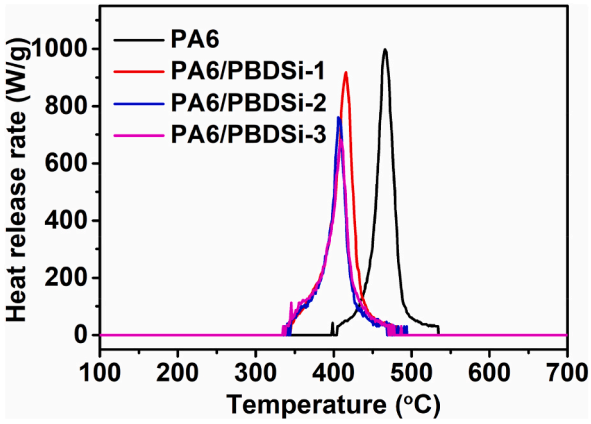

Fig. 5. HRR curves of PA6 and PA6/PBDSi composites.

raising the addition of PBDSi. PA6/PBDSi-3 approaches the THR value of 22.0 kJ/g, much lower than that of PA6 (27.8 kJ/g). These results reveal the positive efficiency of PBDSi as flame retardants for PA6 materials.

3.5. Residues and pyrolysis volatiles analysis

Residue analysis is vital for illustrating the working mechanism of PBDSi in the condensed phase. Firstly, by comparing the digital photos of the residues for PA6 and PA6/PBDSi-3 after burning from Fig. 6(a and b), almost no char remains for PA6 after burning, whereas a black and intumescent char layer is seen for PA6/PBDSi-3. SEM is then performed to monitor the detailed superficial morphologies of the residues, and more complete and denser residues are seen in PA6/PBDSi-3 than PA6 in the corresponding SEM images.

In order to evaluate the graphitization degree of char residues of PA6 and PA6/PBDSi-3, Raman spectra are employed. In Fig. 6(c and d), the Raman spectra of these residues can be divided into two peaks, which are assigned to the G (1571 cm^{-1}) and D (1370 cm^{-1}) bands. As reported [37,38], the graphitization degrees of these residues are then assessed by calculating the integrated intensities ratio of the D to G band (I_D/I_G). The experimental result indicates that the I_D/I_G value of the residues of PA6/PBDSi-3 (1.68) is lower than that of PA6 (2.17), meaning the residues of PA6/PBDSi-3 presents a higher graphitization degree. The higher graphitization degree reflects better thermal stability of residues, which contributes to strengthening the melt-droplets and heat-release suppression behavior of the matrix.

XPS measurements further investigate the detailed chemical structure of the residues of PA6/PBDSi-3, and the relative spectra are displayed in Fig. 6(e and f). In the Si 2p XPS spectrum of residues (Fig. 6(e)), four characteristic peaks at 102.1, 102.7, 103.4, and 103.1 eV are ascribed to the D, T, and Q structures of organic polysiloxane and the stable inorganic SiO_2-like structure, which are generated by the thermal decomposition of polysiloxane units [39,40]. In Fig. 6(f), the P2p XPS spectrum of residues divides into two peaks of P–O–C (134.3 eV) and P–O–P (133.2 eV) that resulted from the formed phosphorus oxides during combustion. To sum up, the above results indicate the generation of a silicon-phosphorous-rich char layer with good thermal stability during the combustion of PA6/PBDSi.

To study the flame-retardant working mode of PBDSi in the gas phase, Py-GC/MS was measured to identify and investigate the pyrolysis products of samples. Fig. 7(a and b) and Tables S1–S2 list the relative chromatograms and main pyrolysis products. Caprolactam and carbon dioxide (CO_2) are two major release volatiles during the pyrolysis process of PA6 and PA6/PBDSi-3. However, the release proportion of caprolactam, a recognized combustible fragment, of PA6/PBDSi-3 during the pyrolysis process is reduced in relation to PA6, indicating that PBDSi inhibits the thermal degradation reaction of the PA6 molecular chain. Moreover, some new silicon-containing fragments with m/z = 222, 296, and 370 g/mol are produced for PA6/PBDSi-3 according to Table S2. These incombustible fragments originating from the polysiloxane unit in PBDSi are conducive to reducing the combustible volatiles concentration during the pyrolysis process.

TG-IR is applied to explore the release evolution of pyrolysis products further evolved from PA6/PBDSi-3 to testify to the positive function of PBDSi in the gas phase. The relevant 3-dimensional TG-IR and the detailed FTIR spectra at different temperatures of pyrolysis products for PA6/PBDSi-3 are recorded in Fig. 7(c and d). Basis on the FTIR spectra, the peaks ascribed to water (3500-4000 cm^{-1}), CO_2 (2360 cm^{-1}), carbonyl (1800-1650 cm^{-1}), and aromatic (1600-1400 cm^{-1}) compounds are observed for PA6/PBDSi-3, owing to the degradation of PA6 backbones [23,41]. As the temperature increases to 430 °C, some organic phosphorus fragments, including P–C, P–O, and P═O stretching vibration in 776, 1096, and 1228 cm^{-1}, are released by the degradation of PBDSi, which play the quenching effect on the gas phase and then promote the carbonization of the matrix [23,42]. Meanwhile, the peak of incombustible NH_3 (969, 930 cm^{-1}) appears, which will help lower the matrix's fire risk by diminishing the combustible gas concentration and the ambient temperature to inhibit the combustion process of the matrix in the gas phase.

In summary, the possible flame-retardant working mode is illustrated in Fig. 8. In the initial pyrolysis stage of PA6/PBDSi composites, H_2O and CO_2 are the two main pyrolysis volatiles. With the increase in temperature, the Schiff base unit in PBDSi will be self-

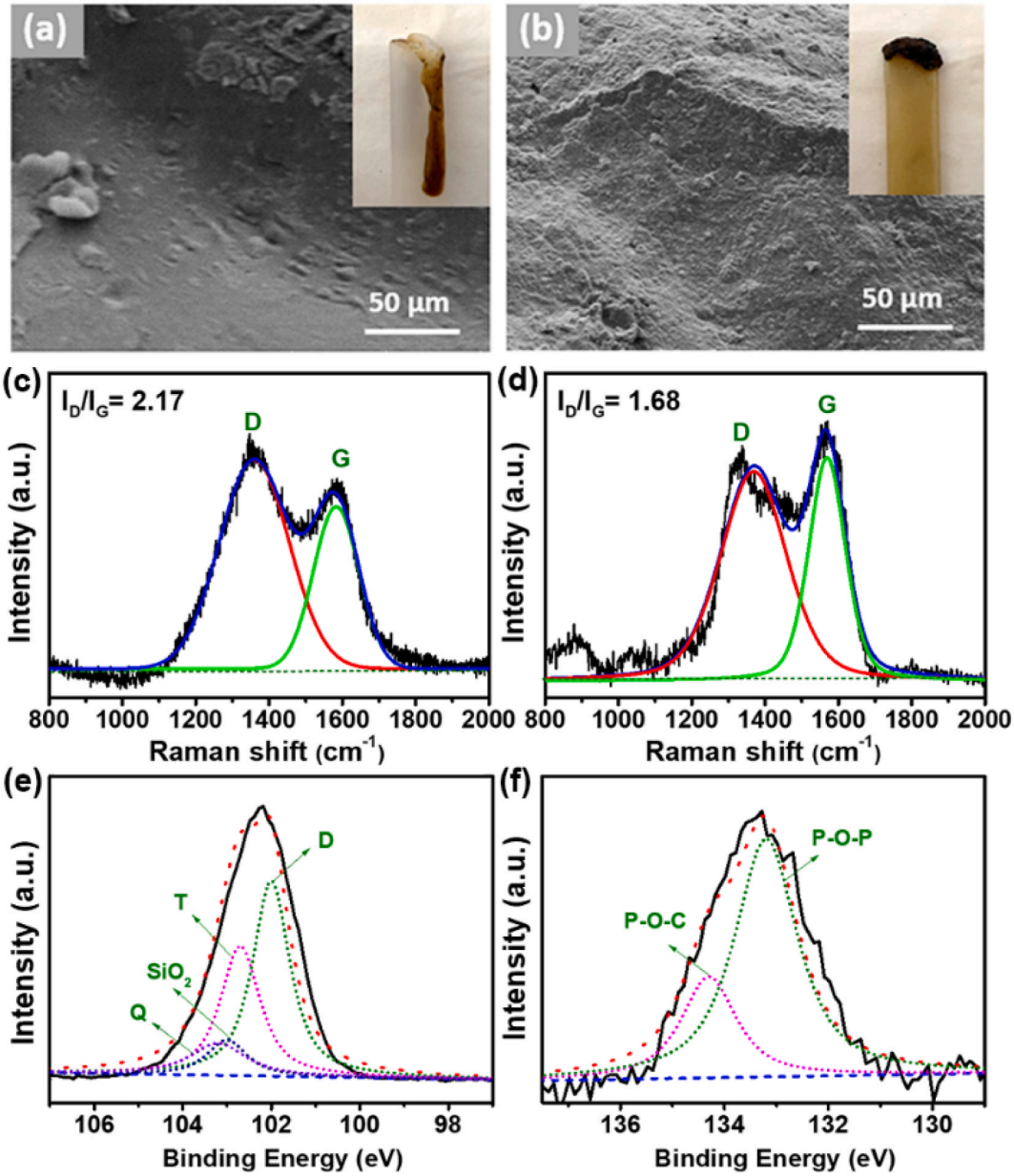

Fig. 6. The digital photos, SEM images (the images near the surface of top edge samples being exposed to the flame) of residues after burning monitored from (a) PA6 and (b) PA6/PBDSi-3. Raman spectra of residues from (c) PA6 and (d) PA6/PBDSi-3. (e) Si 2p, and (f) P2p XPS spectra of the residues of PA6/PBDSi-3.

crosslinked to form a hexatomic ring structure, which is beneficial to inhibiting the thermal degradation process and the melt-dripping behavior of the matrix [16]. As the temperature rises to 430 °C, the PA6 backbone begins to break, and many combustible pyrolysis fragments are released. In this stage, PO· free radicals originating from the phosphorus unit in PBDSi are also released, which can quench the released free radicals from PA6 to suspend the pyrolysis process of PA6 in the gas phase. Meanwhile, the accompanied pyrolysis volatile of NH_3 effectively dilutes the combustible volatiles concentration and further decreases the fire risk of the matrix. In addition, the produced silicon-containing volatiles resulting from the thermal degradation of siloxane unit in PBDSi cooperated with PO· are conducive to forming a stable silicon-phosphorous-rich intumescent char layer. Moreover, inorganic SiO_2 particles with good thermal stability are also formed during this pyrolysis process, further strengthening the intumescent char layer.

4. Conclusions

In this work, a PBDSi is designed via Michael's addition reaction and dehydration-condensation reaction to improve the fire safety

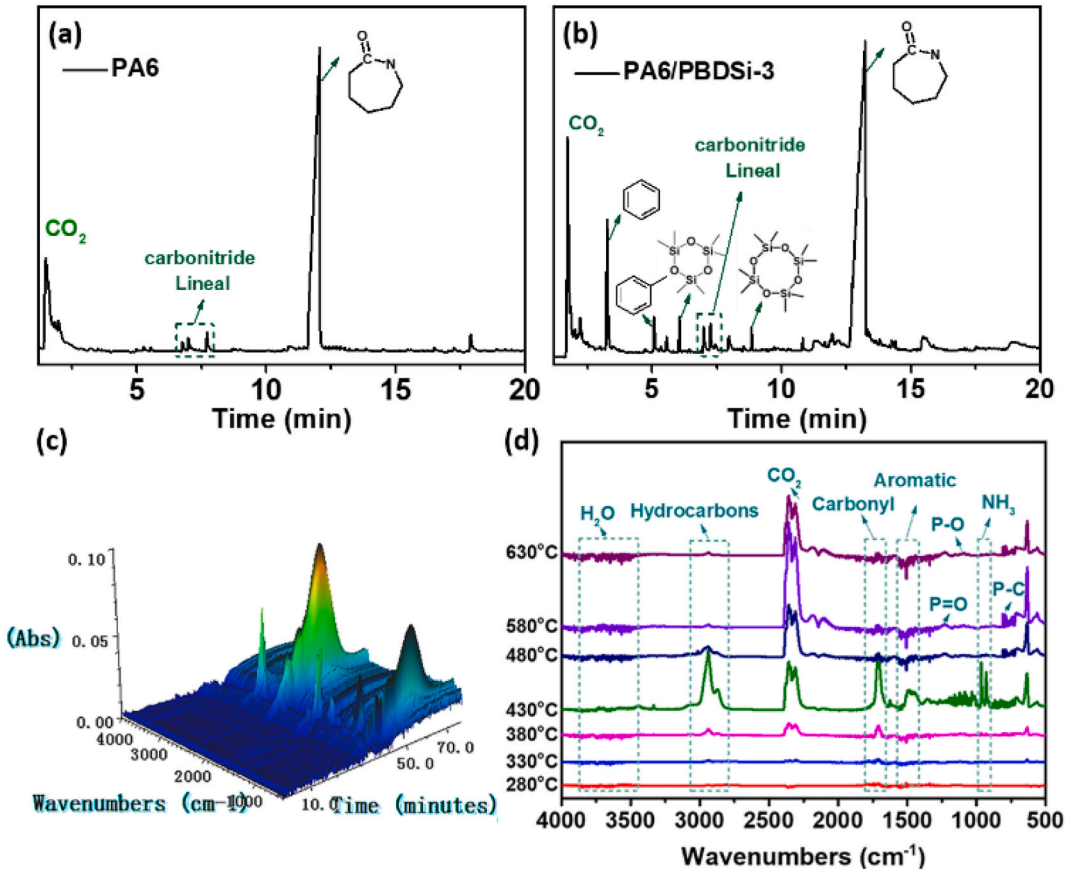

Fig. 7. Py-GC/MS chromatograms of (a) PA6 and (b) PA6/PBDSi-3. (c) 3D TG-IR and (d) the relevant FTIR spectra of pyrolysis volatiles in different temperatures of PA6/PBDSi-3.

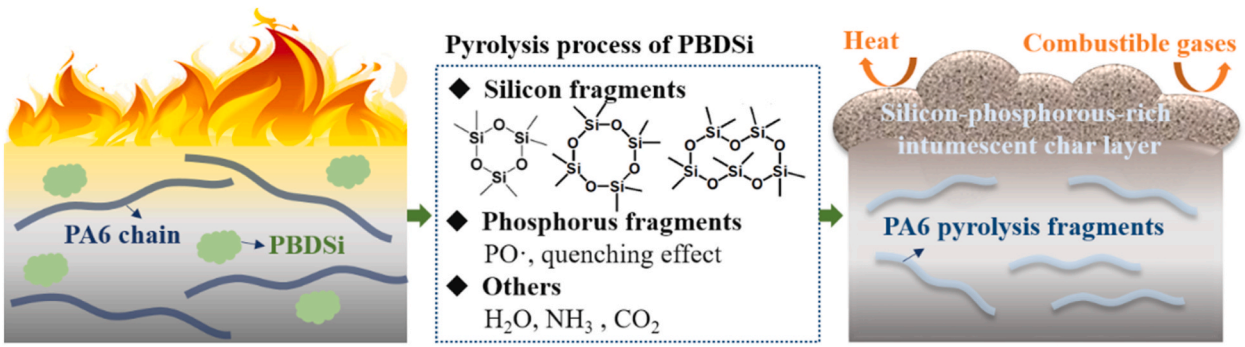

Fig. 8. Possible illustration of the flame-retardant working mechanism.

of PA6. A satisfactory anti-dripping behavior is achieved with a low PBDSi of 3 wt% in PA6 composites. As the PBDSi increases to 5 wt %, PA6/PBDSi-3 attains the LOI value of 27.2 %, while the value of PA6 is only 21.0 %. Meanwhile, the PHRR and THR values of PA6/PBDSi-3 are reduced to 682.2 W/g and 22.0 kJ/g, reducing by about 31.1 % and 20.8 % compared with pure PA6, respectively. The improved fire safety of the modified PA6 originates from the cooperated functions of the generated silicon-phosphorous-rich char layer and released incombustible volatiles of PBDSi. More importantly, a relatively small mechanical loss of PA6/PBDSi is essential for the post-application of PA6.

Data availability statement

Data will be made available on request.

CRediT authorship contribution statement

Shuo Fan: Conceptualization, Formal analysis, Investigation, Supervision, Writing – original draft, Writing – review & editing. **Jinhao Zeng:** Data curation, Methodology, Validation. **Peng Yang:** Data curation, Investigation, Methodology, Software. **Meijia Cheng:** Data curation, Investigation, Validation, Visualization, Writing – original draft.

Declaration of competing interest

The authors declare that they have no known competing financial interests or personal relationships that could have appeared to influence the work reported in this paper.

Acknowledgments

This work is financially supported by the Science Foundation of Zhejiang Sci-Tech University (No.21202088-Y), the National Natural Science Foundation of China (NSFC 52203074), the China Postdoctoral Science Foundation (2023M731331).

Appendix A. Supplementary data

Supplementary data to this article can be found online at https://doi.org/10.1016/j.heliyon.2023.e22877.

References

[1] W. Xiong, L. Chen, D. Wang, F. Song, Y. Wang, Synergistic effects of novolac-based char former with a phosphorus/nitrogen-containing flame retardant in polyamide 6, Chin. J. Polym. Sci. 30 (1) (2011) 72–81.
[2] K. Sha, Y.L. Hu, Y.H. Wang, R. Xiao, Preparation of flame retardant polyamide 6/melamine cyanurate viain situpolymerisation and its characterisation, Mater. Res. Innovat. 18 (2014) 843–847.
[3] K. Fang, J. Li, C. Ke, Q. Hu, K. Tao, J. Zhu, et al., Intumescent flame retardation of melamine-modified montmorillonite on polyamide 6: enhancement of condense phase and flame retardance, Polym. Eng. Sci. 51 (2) (2011) 377–385.
[4] X. Li, L. Shao, N. Song, L. Shi, P. Ding, Enhanced thermal-conductive and anti-dripping properties of polyamide composites by 3D graphene structures at low filler content, Compos. Appl. Sci. Manuf. 88 (2016) 305–314.
[5] W. He, J. Gao, S. Liao, X. Wang, S. Qin, P. Song, A facile method to improve thermal stability and flame retardancy of polyamide 6, Compos. Commun. 13 (2019) 143–150.
[6] M. Lewin, J. Zhang, E. Pearce, J. Gilman, Flammability of polyamide 6 using the sulfamate system and organo-layered silicate, Polym. Adv. Technol. 18 (9) (2007) 737–745.
[7] S. Zhang, X. Fan, C. Xu, P. Ji, C. Wang, H. Wang, An inherently flame-retardant polyamide 6 containing a phosphorus group prepared by transesterification polymerization, Polymer 207 (2020), 122890.
[8] J. Chen, S. Liu, J. Zhao, Synthesis, application and flame retardancy mechanism of a novel flame retardant containing silicon and caged bicyclic phosphate for polyamide 6, Polym. Degrad. Stabil. 96 (8) (2011) 1508–1515.
[9] X. Chen, J. Ye, L. Yuan, G. Liang, A. Gu, Multi-functional ladderlike polysiloxane: synthesis, characterization and its high performance flame retarding bismaleimide resins with simultaneously improved thermal resistance, dimensional stability and dielectric properties, J. Mater. Chem. A 2 (20) (2014) 7491–7501.
[10] S. Fan, C. Zhu, D. Wu, X. Wang, J. Yu, F. Li, Silicon-containing inherent flame-retardant polyamide 6 with anti-dripping via introducing ethylene glycol as the chain-linker and charring agent, Polym. Degrad. Stabil. 173 (2020), 109080.
[11] J. Li, H. Wang, S. Li, A novel phosphorus–silicon containing epoxy resin with enhanced thermal stability, flame retardancy and mechanical properties, Polym. Degrad. Stabil. 164 (2019) 36–45.
[12] P. Jia, H. Liu, Y. Wang, X. Cai, A novel epoxy-functionalized hyperbranched polysiloxane (HPSi) endowing methyl phenyl silicone resin (Si603)/epoxy systems with enhanced compatibility and fire retardancy performance, RSC Adv. 5 (118) (2015) 97413–97421.
[13] L. Zhang, Y. Wang, X. Cai, Effect of a novel polysiloxane-containing nitrogen on the thermal stability and flame retardancy of epoxy resins, J. Therm. Anal. Calorim. 124 (2) (2016) 791–798.
[14] C.-Y. Hsieh, W.-C. Su, C.-S. Wu, L.-K. Lin, K.-Y. Hsu, Y.-L. Liu, Benzoxazine-containing branched polysiloxanes: highly efficient reactive-type flame retardants and property enhancement agents for polymers, Polymer 54 (12) (2013) 2945–2951.
[15] S. Fan, B. Peng, R. Yuan, D. Wu, X. Wang, J. Yu, et al., A novel Schiff base-containing branched polysiloxane as a self-crosslinking flame retardant for PA6 with low heat release and excellent anti-dripping performance, Compos. B Eng. 183 (2020), 107684.
[16] J.N. Wu, L. Chen, T. Fu, H.B. Zhao, D.M. Guo, X.L. Wang, et al., New application for aromatic Schiff base: high efficient flame-retardant and anti-dripping action for polyesters, Chem. Eng. J. 336 (2018) 622–632.
[17] N. Li, J. Ming, R. Yuan, S. Fan, L. Liu, F. Li, et al., Novel eco-friendly flame retardants based on nitrogen–silicone schiff base and application in cellulose, ACS Sustain. Chem. Eng. 8 (2019) 290–301.
[18] J. Sahyoun, V. Bounor-Legaré, L. Ferry, R. Sonnier, A. Bonhommé, P. Cassagnau, Influence of organophosphorous silica precursor on the thermal and fire behaviour of a PA66/PA6 copolymer, Polym. Degrad. Stabil. 115 (2015) 117–128.
[19] F. Liao, L. Zhou, Y. Ju, Y. Yang, X. Wang, Synthesis of a novel phosphorus–nitrogen-silicon polymeric flame retardant and its application in poly(lactic acid), Ind. Eng. Chem. Res. 53 (24) (2014) 10015–10023.
[20] G. Ran, X. Liu, J. Guo, J. Sun, H. Li, X. Gu, et al., Improving the flame retardancy and water resistance of polylactic acid by introducing polyborosiloxane microencapsulated ammonium polyphosphate, Compos. B Eng. 173 (2019), 106772.
[21] Y. Pan, L. Song, W. Wang, H. Zhao, Polydimethylsiloxane wrapped aluminum diethylphosphinate for enhancing the flame retardancy of polyamide 6, J. Appl. Polym. Sci. 137 (35) (2020), 49027.
[22] J. Vasiljevic, M. Colovic, N. Celan Korosin, M. Sobak, Z. Stirn, I. Jerman, Effect of different flame-retardant bridged dopo derivatives on properties of in situ produced fiber-forming polyamide 6, Polymers 12 (3) (2020) 657.
[23] M. Čolović, J. Vasiljević, Ž. Štirn, N. Čelan Korošin, M. Šobak, B. Simončič, et al., New sustainable flame retardant DOPO-NH-functionalized polyamide 6 and filament yarn, Chem. Eng. J. 426 (2021), 130760.

[24] A. Battig, P. Müller, A. Bertin, B. Schartel, Hyperbranched rigid aromatic phosphorus-containing flame retardants for epoxy resins, Macromol. Mater. Eng. 306 (2021), 200073.
[25] P. Chao, Y. Li, X. Gu, D. Han, X. Jia, M. Wang, et al., Novel phosphorus–nitrogen–silicon flame retardants and their application in cycloaliphatic epoxy systems, Polym. Chem. 6 (15) (2015) 2977–2985.
[26] J. Sahyoun, V. Bounor-Legaré, L. Ferry, R. Sonnier, F. Da Cruz-Boisson, F. Melis, et al., Synthesis of a new organophosphorous alkoxysilane precursor and its effect on the thermal and fire behavior of a PA66/PA6 copolymer, Eur. Polym. J. 66 (2015) 352–366.
[27] F.-M. He, B.-W. Liu, L. Chen, D.-M. Guo, X.-M. Ding, Y.-F. Xiao, et al., Novel polyamide 6 composites based on Schiff-base containing phosphonate oligomer: high flame retardancy, great processability and mechanical property, Compos. Appl. Sci. Manuf. 146 (2021), 106423.
[28] Y. Wang, X. Yang, H. Peng, F. Wang, X. Liu, Y. Yang, et al., Layer-by-layer assembly of multifunctional flame retardant based on brucite, 3-aminopropyltriethoxysilane, and alginate and its applications in ethylene-vinyl acetate resin, ACS Appl. Mater. Interfaces 8 (15) (2016) 9925–9935.
[29] Y. Qiu, L. Qian, Y. Chen, J. Hao, Improving the fracture toughness and flame retardant properties of epoxy thermosets by phosphaphenanthrene/siloxane cluster-like molecules with multiple reactive groups, Compos. B Eng. 178 (2019), 107481.
[30] Hawker CJ, Lee R, Frechet JMJ. One-step synthesis of hyperbranched dendritic polyesters. J. Am. Chem. Soc..113(12):4583-4588..
[31] X. Lei, Y. Chen, M. Qiao, L. Tian, Q. Zhang, Hyperbranched polysiloxane (HBPSi)-based polyimide films with ultralow dielectric permittivity, desirable mechanical and thermal properties, J. Mater. Chem. C 4 (11) (2016) 2134–2146.
[32] Y. Zhang, H. Fan, B.G. Li, Synthesis and characterization of advance PA6-b-PDMS multiblock copolymers, J. Appl. Polym. Sci. 131 (22) (2011) 17–24.
[33] T. Kashiwagi, F. Du, J.F. Douglas, K.I. Winey, H.R. Jr, J.R. Shields, Nanoparticle networks reduce the flammability of polymer nanocomposites, Nat. Mater. 4 (12) (2005) 928.
[34] G. Fei, Y. Liu, Q. Wang, Synergistic effects of novolac-based char former with magnesium hydroxide in flame retardant polyamide-6, Polym. Degrad. Stabil. 93 (7) (2008) 1351–1356.
[35] X. Feng, X. Wang, W. Cai, N. Hong, Y. Hu, K.M. Liew, Integrated effect of supramolecular self-assembled sandwich-like melamine cyanurate/MoS_2 hybrid sheets on reducing fire hazards of polyamide 6 composites, J. Hazard Mater. 320 (2016) 252–264.
[36] H. Ge, G. Tang, W.Z. Hu, B.B. Wang, Y. Pan, L. Song, et al., Aluminum hypophosphite microencapsulated to improve its safety and application to flame retardant polyamide 6, J. Hazard Mater. 294 (2015) 186–194.
[37] Y. Zhang, J. Yu, J. Lu, C. Zhu, D. Qi, Facile construction of 2D MXene ($Ti_3C_2T_x$) based aerogels with effective fire-resistance and electromagnetic interference shielding performance, J. Alloys Compd. 870 (2021), 159442.
[38] Z. Yin, J. Lu, X. Yu, P. Jia, G. Tang, X. Zhou, et al., Construction of a core-shell structure compound: ammonium polyphosphate wrapped by rare earth compound to achieve superior smoke and toxic gases suppression for flame retardant flexible polyurethane foam composites, Compos. Commun. 28 (2021), 100939.
[39] R. Wang, D. Zhuo, Z. Weng, L. Wu, X. Cheng, Y. Zhou, et al., A novel nanosilica/graphene oxide hybrid and its flame retarding epoxy resin with simultaneously improved mechanical, thermal conductivity, and dielectric properties, J. Mater. Chem. A 3 (18) (2015) 9826–9836.
[40] F. Hilt, N. Gherardi, D. Duday, A. Berne, P. Choquet, Efficient flame retardant thin films synthesized by atmospheric pressure PECVD through the high Co-deposition rate of hexamethyldisiloxane and triethylphosphate on polycarbonate and polyamide-6 substrates, ACS Appl. Mater. Interfaces 8 (19) (2016) 12422–12433.
[41] T. Liang, J. Cai, S. Liu, H. Lai, J. Zhao, Chain extension and synergistic flame-retardant effect of aromatic schiff base diepoxide on polyamide 6/aluminum diethylphosphinate composites, Materials 12 (14) (2019) 2217.
[42] Y. Zhang, H. Yan, G. Feng, R. Liu, K. Yang, W. Feng, et al., Non-aromatic Si, P, N-containing hyperbranched flame retardant on reducing fire hazards of epoxy resin with desirable mechanical properties and lower curing temperature, Compos. B Eng. 222 (2021), 109043.